Targeted PEGylated Chitosan Nano-complex for Delivery of Sodium Butyrate to Prostate Cancer: An In Vitro Study

Ali Zamanvaziri, MSc[1], Mahboobeh Meshkat, MSc[2],
Soroush Alazmani, MD[3] ⑩, Sepideh Khaleghi, PhD[4] ⑩,
and Mehrdad Hashemi, PhD[1,5]

Abstract

Introduction: Cancer remains a challenging issue against human health throughout the world; As a result, introducing novel approaches would be beneficial for cancer treatment. In this research, sodium butyrate (Sb) is one of the effective anti-cancer therapeutics (also a potent survival factor for normal cells) that was used for prostate cancer suppression in the platform of modified chitosan (CS) nano-complex (polyethylene glycol (PEG)-folic acid (FA)-Sb-CS). **Methods:** Different analytical devices including Fourier transform infrared, dynamic light scattering, high-performance liquid chromatography, scanning electron microscopy, and transmission electron microscopy were applied for the characterization of synthetics. On the other hand, biomedical tests including cell viability assay, molecular and functional assay of apoptosis/autophagy pathways, and cell cycle arrest analysis were potentially implemented on human PC3 (folate receptor-negative prostate cancer) and DU145 (folate receptor-positive prostate cancer) and HFF-1 normal cell lines. **Results:** The quality of the syntheses was effectively verified, and the size range from 140 to 170 nm was determined for the PEG-CS-FA-Sb sample. Also, 75 ± 5% of drug entrapment efficiency with controlled drug release manner (Sb release of 54.21% and 74.04% for pHs 7.4 and 5.0) were determined for nano-complex. Based on MTT results, PEG-CS-FA-Sb has indicated 72.07% and 33.53% cell viability after 24 h of treatment with 9 mM on PC3 and DU145 cell lines, respectively, which is desirable anti-cancer performance. The apoptotic and autophagy genes overexpression was 15-fold (caspase9), 2.5-fold (BAX), 11-fold (ATG5), 2-fold (BECLIN1), and 3-fold (mTORC1) genes in DU145 cancer cells. More than 50% of cell cycle arrest and 45.05% of apoptosis were obtained for DU145 cancer cells after treatment with nano-complex. **Conclusion:** Hence, the synthesized Sb-loaded nano-complex could specifically suppress prostate cancer cell growth and induce apoptosis and autophagy in the molecular and cellular phases.

[1] Department of Genetics, Faculty of Advanced Sciences and Technology, Tehran Medical Science, Islamic Azad University, Tehran, Iran
[2] Department of Biology, Division of Cellular and Molecular Biology, Nourdanesh University of Meymeh, Meymeh, Isfahan, Iran
[3] Student research committee, School of Medicine, Iran University of Medical Science, Tehran, Iran
[4] Department of Biotechnology, Faculty of Advanced Sciences and Technology, Tehran Medical Sciences, Islamic Azad University, Tehran, Iran
[5] Farhikhtegan Medical Convergence Science Research Center, Farhikhtegan Hospital Tehran Medical Sciences, Islamic Azad University, Tehran, Iran

Corresponding Author:
Sepideh Khaleghi, PhD, Assistant Professor of Medical Biotechnology, Faculty of Advanced Science and Technology, Tehran Medical Sciences, Islamic Azad University, Tehran, Iran.
Email: s.khaleghi@iautmu.ac.ir

Introduction

Cancer, as the most significant subject related to human being health, is the leading cause of death around the globe.[1,2] Prostate cancer is the most devastating cancer among men with poor and challenging management during oncology practice. Accordingly, its eradication and at least suppression remain challenging issues throughout the world. Instead, conventional therapeutic approaches such as surgery, chemotherapy, radiation therapy, thermal therapy, etc, which are applied to cancer therapy for decades did not serve as a potential method for prostate cancer inhibition.[3–5] These conventional techniques in cancer therapy owing to their deficiencies like the high side effect, nonspecificity, less cost-effectiveness, poor recovery of patients after treatment, and so on are not efficient.[6] On the other hand, sodium butyrate (Na-OOCCH$_2$CH$_2$CH$_3$: Sb) as a type of natural root bioactive in cancer suppression can apply to the inhibition of various cancers like lymphoma, lung, breast, prostate, kidney, liver, and so forth.[7] Butyrates are naturally occurring short-chain fatty acids that act as a potential energy source, differentiation substance, and survival factor for normal cells[8]; hence, they are completely biocompatible and biodegradable for normal cells. This therapeutic agent can considerably suppress vascular endothelial growth factor (VEGF) through inhibiting histone deacetylases (HDACs) and decreasing VEGFR-mediated angiogenesis and consequently, results in protein kinase B (Akt)-mediated suppression of cell-cycle in the G2/M phase. In the following, reducing the level of Akt, Bcl2, IL6, IL17, and other biomolecules which are involved in angiogenesis and apoptosis can induce programmed cell death in various cancer cells.[9,10] By affecting these functional genes expression, butyrates play a prominent role in the regulation of cell cycle progression, differentiation, apoptosis, and autophagy. Butyrates can also induce autophagy in cancer cells by LKB1/ AMPK signaling pathway. Moreover, it has been reported that butyrate treatment decreases the metastatic capability of cancer cells via suppression of CD44 and pro-MMP-2.[11,12]

As a result, the essential need for finding novel therapeutic techniques such as using nanomaterials as drug delivery systems would be more beneficial for efficient cancer therapy. In the last decades, nanoparticles have been emerging as potential pharmacological devices due to their specific properties such as small sizes, physiochemical characteristics, surface structure, solubility, serum stability, shapes, ease of manipulation, and so forth.[13–16] Moreover, nanoparticles can escape from immune clearance by the lymphocyte-macrophage system, avoid fast clearance of kidney, and as well as ignore liver and lung filtrations due to their surface modifications, size, and structure which, in turn, improve pharmacokinetics and pharmacodynamics of therapeutic agents in the human body.[17] There are 2 types of nanoparticle-based drug delivery systems: passive and active. The passive drug delivery system is based on enhanced permeability and retention (EPR) effects in which drug-loaded nanocarrier can penetrate cancer sites through uneven endothelium of blood vessels in tumor tissue since vasculatures are irregular in shape and leaky.[18]

Furthermore, in active drug delivery systems, nanodevices can uptake in tumor cells via receptor-mediated internalization which is also known as targeted drug delivery systems. Ligand-decorated nanoparticles are involved in active therapeutic delivery systems against receptors of specific cancer cells.[19]

Among various nanomaterials, polymeric nanoparticles such as chitosan (CS) because of different remarkable characteristics, including enhancing drug half-life in human serum, high drug loading capacity, sustained and controlled bioactive release, avoiding enzymatic degradation, suitable biodegradability and biocompatibility, ignoring immune system cells, etc are considered as a promising candidate for efficient bioactive delivery to tumor cells and cancer therapy.[20,21] In addition, functional surface amino groups of CS nanoparticles lead to providing an opportunity for potential surface functionalization and modification which plays a prominent role in improving aspects of CS nanoparticles such as getting away from immune clearance by the lymphocyte-macrophage system and clearance of kidney, and pharmacokinetics and pharmacodynamics.[22] For instance, surface modification of CS with polyethylene glycol (PEG) biopolymer can further increase various aspects of nanocarrier like biocompatibility and biodegradability, serum stability, EPR effect, controlled drug release, etc.[23,24] Furthermore, the surface amino groups can be potentially involved in the conjugation of biomolecules for targeting nanocarriers to cancer sites. By functionalization of nanoparticles with targeting agents like an antibody, aptamer, peptide, folic acid (FA), and so forth, active drug delivery systems can be fabricated which is in favor of novel nanoparticle-based devices in cancer prognosis, diagnosis, and therapy.[25] FA due to its specificity towards FA-receptors, good conjugating properties, ease to access, inexpensive, nonimmunogenicity, facilitating EPR effect, high serum stability, biodegradability, biocompatibility, and so on, is an efficient biomolecule for site-specific cancer therapy.[26,27] FA-receptors have a high expression on the surface of various tumors such as breast, liver, kidney, prostate, etc, which significantly improve targeted internalization of nano-conjugate to target cells.

Herein, we effectively developed PEG-modified and FA-functionalized CS-based nano-complex for the targeting delivery of Sb to various prostate cancer cells. This combination is new and there aren't any similar samples. While Sb can have an effective role in cancer inhibition in combination with targeted and biocompatible structure can be more effective and safe for in vivo application. After the synthesizing of PEG and FA conjugated nano-complex and drug loading, several analytical devices such as Fourier transform infrared (FT-IR), dynamic light scattering (DLS), scanning electron microscopy (SEM), and transmission electron microscopy (TEM) were applied to the qualification and quantification of synthetics. Then, the drug loading efficiency and drug release manner of the PEG-CS-FA-Sb sample were measured quantitatively by high-performance liquid chromatography (HPLC). Subsequently, in vitro biomedical tests, including cell viability, a molecular and functional assay of apoptosis /autophagy pathways, and cell cycle arrest analysis were potentially

implemented on human PC3 (FA receptor-negative) and DU145 (FA receptor-positive) prostate cancer cell lines and HFF-1 as normal cell line for evaluating the prostate cancer cells' inhibition potency of synthetics.

Materials and Methods

Reagents and Apparatus

CS (Mw: 50 000 to 190 000 Da; Viscosity: 20 to 300 cp; CAS Number: 9012-76-4), NH2-PEG20K-COOH, HCl salt (Mw: 20 000 Da; CAS number: jka5160), FA (Mw: 441.4 g/mol; CAS number: 59-30-3), Sb ($\geq$ 98.5% GC; molecular weight: 110.09 g·mol^{-1}; CAS number: 156-54-7) tripolyphosphate (TPP, CAS number: 7758-29-4), 1-ethyl-3-(3-dimethyl-amino-propyl) carbodiimide (EDC, CAS number: 25952-53-8), N-hydroxysuccinimide (NHS, CAS number: 6066-82-6), di-methyl-sulphoxide (DMSO, CAS number: 67-68-5), and cellulose dialysis membranes were obtained from Sigma Aldrich. The 3-(4,5-dimethylthiazol-2-yl)-2,5-diphenyltetrazolium bromide (MTT), the RPMI 1640 medium, Dulbecco's Modified Eagle Medium (DMEM), and fetal bovine serum (FBS) were also bought from Sigma-Aldrich. The DU145, PC3 prostate cancer cell, and HFF-1 normal cell lines were obtained from the Institute of Pasteur, Iran.

Spectroscopic evaluations of syntheses were carried out by applying an FT-IR spectrometer (Perkin-Elmer 843), and HPLC. The SEM and TEM images were taken through Philips EM 208S (the Netherlands), and the DLS technique was performed via NanoBrook 90 Plus (Brookhaven, USA).

Synthesis of PEG-CS

In this step, NH2-PEG-COOH was conjugated to surface-modified CS by esterification reaction with NHS and EDC which led to the formation of an amide bond between the PEG amine group and modified CS. To synthesize PEGylated-CS, the CS solution was prepared by dissolving 80 mg of CS in 2 mL of acetic acid 1% under vigorous stirring at room temperature for 5 h. Then, a PEG solution was provided using EDC/NHS. 7.6 mg of PEG was added to 20 mL of the prepared mixture of EDC (0.4 mM)/NHS (0.1 mM) solution and stirred at 60 rpm at room temperature for 4 h. This reaction was implemented at dark and nitrogen atmosphere conditions. Then, the prepared solutions were mixed and 1 mM of NaOH was added to the mixture drop by drop under stirring conditions to obtain PEG-CS precipitation.

Synthesis of PEG-CS-FA

In this phase, FA as a targeting agent was conjugated to surface-modified CS by esterification reaction with NHS and EDC which led to the formation of an amide bond between the FA and modified CS. This conjugation was carried out as follows the procedure. Firstly, 280 mg of FA was solubilized in EDC/NHS solution (1:1 molar ratio) and stirred at 80 rpm for 3 h under light-protected and nitrogen circumstances. Secondly, the prepared PEG-CS copolymer solution in 10 mL of acetic acid 1% was added to the prepared FA solution, and the reaction was incubated at 70 rpm of stirring and room temperature overnight. This reaction was also implemented in dark conditions and a nitrogen atmosphere. Then, the pH of the solution was neutralized using NaOH. Eventually, to obtain the globular nano-complex, 1 mL of TPP 0.5% was added to the prepared PEG-CS-FA solution drop by drop under ultra-sonication conditions. After that the precipitated PEG-CS-FA was ultracentrifuged at 15 000 rpm for 20 min. The supernatant containing free PEG and FA was removed and replaced by a fresh phosphate buffer saline (PBS) buffer. The monodispersed nano-complex would be achieved by ultra-sonication. The absorbance of free FA concentration was calculated by measuring 256 nm and the concentration was evaluated by standard curve. The efficiency of FA conjugation was calculated according to the below formula:

$$\text{Conjugation efficiency}(\%) = \frac{\text{Conjugated FA Con. (Total FA con. } - \text{ Free FA Con.)}}{\text{Total FA Con.}} * 100$$

The conjugation efficiency of FA was about 60 $\pm$ 10%.

Drug Loading into PEG-CS-FA

In this part, a certain amount of Sb was suspended in the ionized water and drug loading was performed in an aqueous solution. Briefly, 30 mg of the Sb was dissolved in 8 mL of deionized water under stirring at 70 rpm for 3 h to obtain a homogenous solution. Then, the drug-containing solution was added to 5 mL of PEG-CS-FA at room temperature, and the solution was stirred at 90 rpm for 10 h. Thereafter, 1 mL of TPP was slowly added to the drug-containing solution under ultra-sonication conditions. Afterward, the drug-loaded nano-complex was ultracentrifuged at 15 000 rpm for 20 min for drug entrapment efficiency assessment. The supernatant containing free Sb was lyophilized for considering the Sb concentration by HPLC. For cellular and analytical experiments, the drug-loaded nano-complex was transferred to a dialysis tube and free drugs were separated by dialyzing in 1000 mL of the PBS buffer (pH 7.4) at room temperature on a magnetic stirrer for 30 min. Dialysis was also repeated with deionized water 3 times.

Characterization of Synthetics

Various analytical techniques were applied for the qualification and quantification of synthetics. FT-IR spectroscopy was used for the qualification of conjugates. The FT-IR spectra of the synthesized nanocomposites were conducted utilizing the KBr pellets strategy at diffuse reflectance mode of 4 cm^{-1} within the extend 400–4000 cm^{-1}. For more characterizations, the DLS gadget was connected to find out the hydrodynamic molecule estimate and the surface charge of the nanocomposites. These tests were measured at 25 ± 1 °C utilizing weakened specimens. The zeta potential of nanocomposites was evaluated by a zeta sizer. Each test was exhausted triplicate. In addition, the molecule measure and dispersity of the nanocomposites were examined through TEM. The naturally arranged suspensions of the nanocomposites were scattered onto a copper framework which proceeded by its drying at 25 °C. After the retention of additional water particles by channel paper, the specimen's microphotographs were taken at a quickening voltage of 120 kV. On the other hand, the surface morphology and dispersion of tests were overviewed by applying an SEM. Also, HPLC was employed for the quantification analyses of specimens.

Drug Entrapment Efficiency

To the measurement of drug-loading rate into PEG-CS-FA nano-complex, 5 mg lyophilized supernatant, containing free Sb in the 2.4 section, was dissolved in 1 mL of methanol, and the Sb values in the solution were ascertained by HPLC. This measurement was carried out by applying a C18 column (5 μm, 250 mm × 4.6 mm) and using methanol and 0.1% acetic acid (88:12) (v/v) as mobile phase. The flow rate was considered 1.0 mL/min. The ultraviolet detector wavelength was 480 nm and the injection volume was 30 μL. The entrapment efficiency was calculated according to the below formula:

$$\text{Entrapment efficiency (\%)} = \frac{\text{Entrapped Sb con. (Total Sb con.} - \text{Free Sb Con.)}}{\text{Total Sb Con.}} * 100$$

Drug Release Study

The in vitro drug release behavior of PEG-CS-FA-Sb synthetics was scrutinized in PBS as a simulation of real release medium at pHs 7.4 and 5.0 under 37 °C.[28] Briefly, 2 mg of PEG-CS-FA-Sb nano-complex was suspended in 4 mL of PBS and spilled in the prepared dialysis membrane. Thereafter, the dialysis tube was immersed in 100 mL of PBS at a backer, and the container was placed in an incubator-shaker set at 60 rpm at 37 °C. Afterward, 150 μL of the release medium was gathered at regular intervals of time by 64 h, and the removed release medium was again substituted with fresh PBS at all times. Then, collected specimens were assessed (n = 3) according to the free drug calibration curve using an HPLC device at a wavelength of 480 nm.

Cell Culture

The human PC3, DU145 prostate cancer, and HFF-1 normal cell lines were purchased from the Pasture Institute of Iran. These cell lines were separately cultured in the RPMI medium supplemented with 10% FBS, 2 mM glutamine, 100 μg/mL streptomycins, and 100 IU/mL penicillin for cellular assessment.

Cell Viability Assay

3-(4,5-dimethylthiazol-2-yl)-2, 5-diphenyl tetrazolium bromide (MTT) assay is applied to evaluate the cytotoxicity synthetics including PEG-CS, PEG-CS-Sb, PEG-CS-FA, and PEG-CS-FA-Sb nano-complexes, on prostate cancer cells (PC3, DU145, and HFF-1) after 24, 48, and 72 h of treatment. To achieve this, relatively 1 × 10^4 cells/well of (96 well plates) were seeded and incubated at 37 °C and 5% CO$_2$ for 24 h. Next, the nano-complexes were prepared in a serum-supplemented tissue culture medium which was followed by sterilizing through a 0.2 mm filter at pH 7.4. After incubation, the culture medium was substituted via an equal amount of new medium containing various concentrations (1.125, 2.25, 4.5, and 9 mM) of PEG-CS, PEG-CS-Sb, PEG-CS-FA, and PEG-CS-FA-Sb samples. The Sb concentrations in PEG-CS-Sb and PEG-CS-FA-Sb treatments are 20, 10, 5, 2.5, and 1.25 mM. After mentioned times, the medium of sample-treated wells was replaced by 200 μL RPMI without serum, and 15 μL of sterile-filtered MTT salt was solubilized in PBS pH 7.4 (5 mg/mL) and added to each well at 0.5 mg MTT/mL final concentration. The plate was incubated for 4 h. Afterward, the suspension liquid was collected and the cells were re-suspended in DMSO and optical density (OD) was read at 570 nm using an ELISA reader (Bio-Rad Instruments Inc., USA). The difference in OD of the treated and nontreated cells was applied for the calculation of cell viability. All experiments were repeated 3 times.

Gene Expression Study

The quantitative expression of genes involved in apoptosis (Caspase 9, BAX) and autophagy (ATG5, BECLIN1, mTORC1) were measured via quantitative real-time PCR (qRT-PCR) technique. Briefly, prostate cancer cells were

seeded in 6-well plates (1×10^6 cells/well) and incubated for 24 h at 37 °C and 5% CO_2, and the cells were treated with IC_{50} concentrations of PEG-CS, PEG-CS-Sb, PEG-CS-FA, and PEG-CS-FA-Sb nano-complexes which were followed by further incubation for 24 h. Thereafter, the RNA of the sedimented trypsinized prostate cancer cells was isolated by submerging them in RNX-PLUS solution and 200 μL of chloroform. After centrifugation of cells and collecting the supernatant, isopropanol solution was added to the cell-containing vial, the cells were centrifuged again, and precipitation was immersed in 1 mL of ethanol 75%. Next, 1000 ng of high-quality RNA was utilized for cDNA synthesis by the reverse transcription process as the following content: 10 μL of master mix real-time, 3 μL (10 ng) RNA, and 7 μL double distilled water. The qRT-PCR test was performed with a 14 μL of the reaction mixture, 1 μL of cDNA, 7 μL of low Rox master mix real-time, and 0.5 μL of forwarding primer (Caspase-9: 5′-TGGCTCCTGGTACGTTGA-3′; Bax: 5′-TTT CTGACGGCAACTTCAACTG-3′; ATG5: 5′-CATTCAGAA GCTGTTTCGTCCT-3′; BECLIN1: 5′-GATGATGTCCACA GAAAGTGC-3′; mTORC1: 5′-CTGATTCTCACAACCCA GCG-3′) and 0.5 μL of reverse primer (Caspase-9: 5′-GAAA CAGCATTAGCGACCCT-3′; Bax: 5′-TCCAATGTCCAG CCCATGA-3′; ATG5: 5′-CTCAGATGTTCACTCAGCCA C-3′; BECLIN1: 5′-AGTGACCTTCAGTCTTCGG-3′; mTORC1: 5′-ATCATCCCGATTCATGCCCT-3′) and the PCR temperature was set up by RT-qPCR device as the following: heating at 95 °C for 10 min, 45 cycles at 95 °C for 15 s, annealing at 59 °C for 25 s, and elongation at 72 °C for 30 s. Finally, the gene expression amounts were normalized to glyceraldehyde-3-phosphate-dehydrogenase (GAPDH) for measuring the fold change in gene expression relative to the control.

Cell Cycle Arrest Assay

PC3 and DU145 prostate cancer cells (1×10^6 cells/mL) were grown in a 6-well plate and incubated at 37 °C and 5% CO_2 for 24 h.[29] Then, cultured cells were treated with IC_{50} concentrations of PEG-CS-FA-Sb to evaluate the effect of the nano-complex on the cell cycle distribution. After 24 h of incubation, the media of plate wells were removed and the PEG-CS-FA-Sb nano-complex prepared in the culture medium was added to the wells, and the plate was incubated for a further 5 h. In the following, the treated cells were trypsinized, washed with PBS, and fixed in 75% ethanol for 30 min. The cancer cells were suspended in PBS with 50 μg/mL propidium iodide (PI) and 0.1 mg/mL RNase-A at 4 °C and light-protected conditions for 40 min. Eventually, after washing with cold PBS and shaking at 37 °C, the cell cycle arrest was analyzed using flow cytometry.

Apoptosis Assay

Flow cytometry was used to examine apoptosis values of the conjugate in PC3 and DU145 cancer cells. Briefly, 1×10^6 cells/mL cancer cells were grown in 6-well plates. After 24 h of incubation at 37 °C and 5% CO_2, the cells were treated with IC_{50} concentrations of PEG-CS-FA-Sb nano-complex prepared in a fresh medium. After 5 h of incubation, the cancer cells were detached using trypsin, washed with PBS 3 times (to remove trypsin and extra PEG-CS-FA-Sb), and then resuspended in 1 mL of PBS. Next, after centrifugation at 1000 rpm for 2 min to collect cancer cells, the cancer cells were stained with the Annexin V-FITC and PI dye and incubated at dark conditions for 15 min. Ultimately, prostate cancer cells were exposed to the flow cytometry device to calculate apoptotic cells.

Statistical Analyses

Data are expressed as mean ± SD. The statistical analyses were carried out using one-way ANOVA and T-test (Graph Pad Prism 8 software). Values of $P < .05$ were considered significantly different from the controls.

Results and Discussion

Characterization of Synthetics

FT-IR Analysis. FT-IR spectroscopy was employed to approve the quality of CS nano-complex and its derivatives (Figure 1). As depicted, the absorption peaks of the free CS sample (Figure 1A) were attained at around 3448, 3423, 3339, 1157, and 1030 cm^{-1} which are related to $-NH_2$ and $-OH$ groups stretching vibration, O–H and N–H stretching vibrations, asymmetric stretching of $-C-O-C-$ bridge, and C–N bond, respectively.[30] Moreover, characteristic peaks at around 1423 cm^{-1} and between 2800 and 3000 cm^{-1} are attributed to the C–H stretching in methyl groups and CH, CH_2, and CH_3 stretching vibrations in the pure CS nanoparticle, respectively. CS also demonstrated absorption peaks at around 1645 cm^{-1} (C = O), 1363 cm^{-1} (C–N stretching), and 1085 cm^{-1} (C–O stretching).[18,31] For the PEG-CS sample (Figure 1B), the peaks at around 1364, 1405, and 3150 cm^{-1} are owing to –C = O stretch, C = O stretch of carbonyl group, and C–H stretch, respectively. In addition, absorption peaks at about 644 cm^{-1} (CH_2 rocking), 1020 cm^{-1} (C–N stretching), and 1647 cm^{-1} (NH–C = O stretching of amide bond) are indicative of PEG-CS.[32] Besides, the main FT-IR characteristic peaks of FA in the compartment of PEG-CS-FA conjugate (Figure 1C) were revealed at around 3446 and 3420 cm^{-1} due to N–H stretch of primary amine and amide, 3320 to 3500 cm^{-1} for the presence of alkyl C = H and C–C stretch, 1695 cm^{-1} owing to aromatic C–C bending and stretching, and 1460 to 1490 cm^{-1} because of amides bend formation.[18] Besides, the peak at around 1728 cm^{-1} is indicative of the C = O stretching of Sb in the PEG-CS-FA-Sb nano-complex. The peak shift in a spectrum of 2850 to 2980 cm^{-1} could also be due to the C–H stretch of the Sb drug.

DLS, Zeta Potential, and Microscopic Analyses. The particle size plays a significant role in the efficient delivery of drug agents to cancer cells since the physicochemical and biomedical performance of nanocarrier such as stability, escaping from the immune system, drug loading capacity, pharmacokinetics and
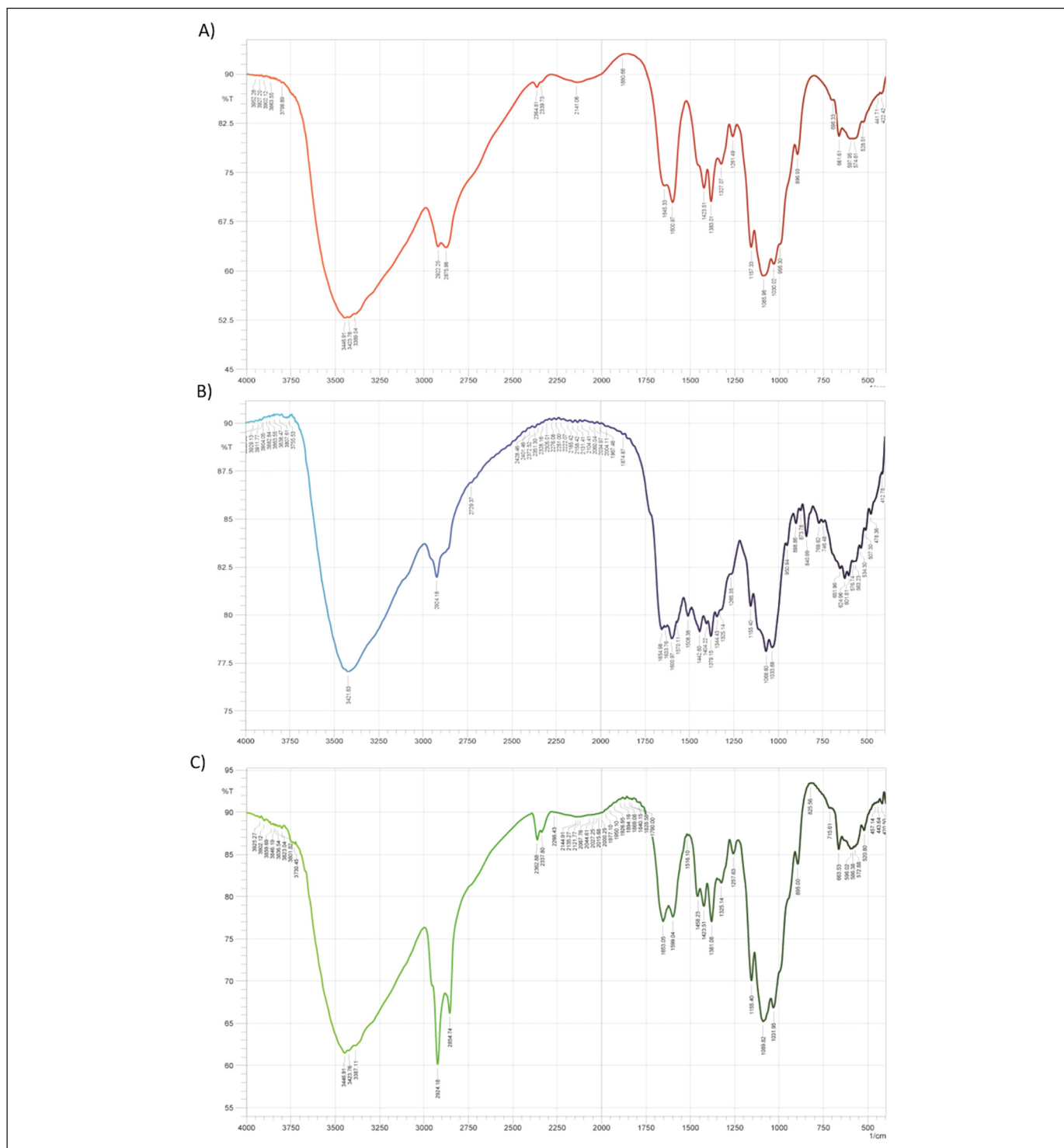
Figure 1. The FT-IR spectra of CS (A), PEG-CS (B), and PEG-CS-FA (C). The absorption peaks are showing the appropriate surface modification, surface functionalization, and drug loading into CS nanoparticle sand to verify the efficient qualification of syntheses. For pure CS nanoparticles, the absorption peaks were determined at around 3448, 3423, and 3339 cm^{-1} which is related to –NH$_2$ and –OH groups stretching vibration, O–H and N–H stretching vibrations, asymmetric stretching of –C–O–C– bridge, respectively. The characteristic peaks at about 1364 and 1405 cm^{-1} are indicative of the –C = O stretch and C = O stretch of the carbonyl group in the structure of PEG-CS. For, PEG-CS-FA nano-conjugate the peaks at around 3446 and 3420 cm^{-1} are attributed to the N–H stretch of primary amine and amide. Also, Sb bioactive in the compartment of PEG-CS-FA revealed the absorption peak at around 1728 cm^{-1} due to C = O stretching.
Abbreviations: CS, chitosan; PEG, polyethylene glycol; FA, folic acid; FT-IR, Fourier transform infrared.

pharmacodynamics, values of drug dosage, and effective therapeutic efficiency, are directly relevant to the particle size.[33] As a result, the particle size and topology of nano-complexes were determined via DLS, SEM, and TEM. According to DLS results, the hydrodynamic size of pure CS and PEG-CS nano-complex were earned about 88.0 and 96.7 nm (PDI: 0.27) which confirms the successful conjugation of PEG to CS and suitable size of nanocarrier after its modification. After the conjugation of FA to PEG-CS nano-complex, the hydrodynamic diameter reached a size of 99.7 nm (PDI: 0.25). These data verify the covalent conjugation of PEG and FA and potentially show the favorable size of nanocarrier for delivery of bioactive to cancer cells. Additionally, the drug-loaded compartment indicated a sharp growth in diameter (211.0 nm, PDI: 0.29) which could be owing to the formation of the hydrogenic bond between the surface functional groups of CS and Sb. On the other hand, the TEM (Figure 2A) and SEM (Figure 2B) images were taken to investigate the exact size, shape, dispersion, and morphology of the main specimen (PEG-CS-FA-Sb). The zeta potential of PEG-CS, PEG-CS-Sb, PEG-CS-FA, and PEG-CS-FA-Sb were 15 ± 1.8, 10 ± 1.3, 8 ± 1.6, and 5 ± 2.1 mV, respectively. Based on SEM and TEM results, the nano-complex has demonstrated a globular shape and narrow particle size with a spectrum of 100 to 150 nm which is desirable for the delivery of therapeutics to tumor sites. As reported, the nano-complexes with a size < 200 nm have appropriate distribution in cancer tissues because of the lack of unity in the formation of the vasculatures in cancer tissues which is the result of fast growth in them.[34] Furthermore, nanocarriers with a size range of 70 to 200 nm could easily disperse in the whole human body through the circulatory system, and effectively facilitate the EPR effect which is crucial for the cellular uptake of drug-content nanoparticles.[15,35]

Drug Entrapment Efficiency and Drug Release Study

The entrapment efficiency of Sb in CS nano-complex was measured according to the standard curve, and it was about 75 ± 5%. This value of Sb entrapment is suitable for CS nano-complex, and the surface modifications of CS had probably an effect on the efficiency of drug entrapment. This level of drug entrapment efficiency using a cost-effective preparation approach for biocompatible and biodegradable CS nano-complex would be more beneficial since this subject is considered the main aspect of delivery systems.[36] Also, the drug release manner of synthetics was scrutinized in PBS under pHs 7.4 and 5.0 at 37 °C (Figure 3). Based on the HPLC outputs, the nano-complex had controlled release in normal pH than acidic pH. A 14.75% of Sb release was observed within the first 3 h in PBS for normal pH while it was 24.59% for pH 5.0 at the same time. Moreover, total Sb release was attained at 54.21% and 74.04% for pHs 7.4 and 5.0 at the end of the period, respectively, which expresses rapid drug in an acidic medium. Rapid drug release is desirable in cancer sites since their medium has acidified microenvironment. The endosomes have also acidified pH values and fast drug release can lead to potential apoptosis-inducing in cancer cells.[28] The controlled Sb release could be due to the presence of intermolecular and intramolecular interactions like the hydrogen-bonding, electrostatic interactions, and π–π interactions. Besides, CS nano-complex chains protonate in the acidic pH which leads to the unfolding of CS and drug release in the acidic tumor microenvironment.[37,38] These data have been exhibiting the potential capability of CS nanoparticles in the efficient delivery of therapeutics to cancer cells without considerable side effects on body normal cells. Our outputs are approximately in line with the findings of Xie et al[39] in which they developed a doxorubicin-loaded CS-PEG nano-complex as a controlled delivery system. According to their data, CS-based nanocarrier had been demonstrated a more controlled release manner than our formulation in neutral pH while the fast release was determined in our and their works in acidic pH. This comparison has been showing the appropriate release behavior of CS-based nano-complexes in cancerous tissues.
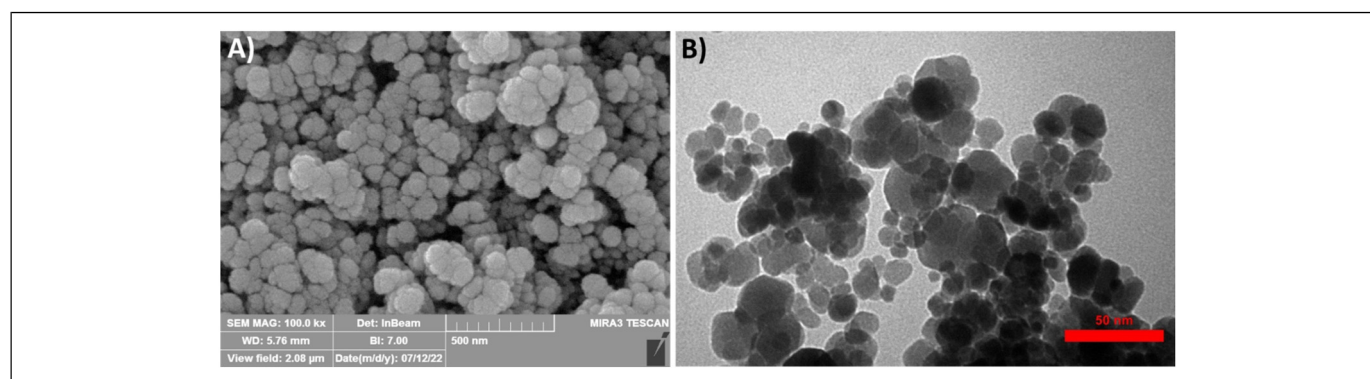

Figure 2. SEM (A) and TEM (B) images of PEG-CS-FA-Sb nano-complex. These images are showing the nano-size with globular structures and shapes. The size range of 100 to 150 nm was attained for the nanocarrier. This size range is suitable for the dispersion of nano-complex in cancer tissues because of the lack of unity in the formation of the vasculatures in cancer sites.
Abbreviations: CS, chitosan; PEG, polyethylene glycol; Sb, sodium butyrate; FA, folic acid; SEM, scanning electron microscopy; TEM, transmission electron microscopy.

Figure 3. The drug release profile of PEG-CS-FA-Sb nano-complex at pH values of 7.4 and 5.0. Nanocarrier indicates a controlled Sb release behavior at physiologic pH (7.4) than acidified pH (5.0). The main cause of release in acidified pH is the protonation of the CS chains which results in a fast Sb release ratio. This fast drug release is significantly suitable for cancer therapy since the environments of cancer cells and as well as endosomal organelles are acidified.
Abbreviations: CS, chitosan; PEG, polyethylene glycol; Sb, sodium butyrate; FA, folic acid.

Cell Viability Assay

Cell cytotoxicity studies of synthetics (PEG-CS, PEG-CS-Sb, PEG-CS-FA, PEG-CS-FA-Sb) were carried out applying MTT assay with the human PC3 (FA-receptor negative) and DU145 (FA-receptor positive) prostate cancer and HFF-1 normal cell lines. This test was performed with different concentrations of samples, including 1.125, 2.25, 4.5, and 9 mM, at 24, 48, and 72 h of posttreatment. The results have exhibited that drug-containing samples had a higher cytotoxic effect on cancer cell lines than others; the surface-modified samples, likewise, indicated lower toxicity in comparison to Sb-loaded specimens. Moreover, FA-functionalized nano-complexes have revealed negligible toxicity due to efficient internalization in DU145 (FA-receptor positive) cancer cell line than PC3 (FA-receptor negative) cancer cells and HFF-1 cells. As indicated in Supplemental Figure S3A, the momentous cytotoxicity was observed for the PEG-CS-FA-Sb nano-complex on DU145 cells (20.13% of cell viability) after 48 h of treatment with 9 mM concentration. The cell viability value for 9 mM concentration at 24 h (Figure 4C) and 72 h (Supplemental Figure S3B) of posttreatment was about 33.53% and 45.22%, respectively, while it was only 72.07% and 78.17% for PC3 cancer cells (Figure 4B and Supplemental Figure S2B) and 71.1% and 61.0% for normal cells (Figure 4A and Supplemental Figure S1) at the same time. These data have been demonstrating that the PEG-CS-FA-Sb nano-complex can effectively internalize into cancer cells through FA-receptor and induce cell death by blocking various critical molecules in cancer cells such as inhibition of histone deacetylases and protein kinase B (Akt) in the G2/M phase of cancer cells cycle.[26,27] In comparison to the PEG-CS-FA-Sb nano-complex, the cell viability values for the nontargeted sample (PEG-CS-Sb) were shown slight toxicity, 66.78% and 61.3% cell viability for DU145 (Figure 4C and Supplemental Figure S3) and

61.08% and 60.18% cell viability for PC3 (Figure 4B and Supplemental Figure S2) cell lines after 24 and 48 h of treatment with 9 mM concentration, respectively, which further approves nontargeted delivery of Sb.[16,21] Additionally, pure PEG-CS and PEG-CS-FA nano-complex did not have considerable toxicity on DU145, PC3, and HHF-1 cell lines and even improved the growth of cells as nutrition. This biocompatibility is mainly due to PEG and FA biomolecules which facilitate the excellent performance of nanocarriers in drug delivery systems. Furthermore, the 50% maximal inhibitory concentration (IC_{50}) of formulations was obtained at 9 mM (after 24 h of treatment) and 1.125 mM (after 48 h of treatment) for PEG-CS-FA-Sb nano-complex treated on DU145 cells (Figure 4C and Supplemental Figure S3). These outputs have been depicting that PEG-CS-FA-Sb nano-complexes could be a potential candidate for efficient drug delivery to cancer cells. The results are also inconsistent with research work by Khan et al[40] in which FA-CS nano-complex has been applied to the targeting delivery of bioactive to ovarian and breast cancer cells. Compared with Xie et al[39] research in which they used nontargeted CS-PEG nano-complex for delivery of doxorubicin to cancer cells, our synthetics have indicated better prostate cancer cell inhibition performance than their nano-complex which could be due to FA-receptor-mediated internalization of CS-FA-PEG-Sb nano-complex therapeutics. Moreover, Sb as a kind of natural anticancer drug could be suppressed cancer cell growth more efficiently; hence, this drug is a promising candidate for the inhibition of cancer cells, even in vivo investigations. In another work by Inphonlek et al,[41] the CS/carboxymethylcellulose-stabilized poly(lactide-co-glycolide) nano-complex has been conducted for effective delivery of curcumin (bio-drug) to HCT 116 cells. Their data same as our findings have revealed suitable cancer cell growth suppression potency although the performance of our synthetics was more reliable for cancer cell inhibition than theirs.

Gene Expression Study

In vitro gene autophagy (ATG5, BECLIN1, mTORC1) and apoptotic (Caspase9, BAX) gene expressions were examined by the qRT-PCR analysis, and data are demonstrated in Figure 5. To achieve this, human PC3 and DU145 prostate cancer cells were treated with IC_{50} concentration (9 mM) of PEG-CS-FA-Sb as well as 9 mM concentrations of PEG-CS, PEG-CS-Sb, PEG-CS-FA nano-complexes. The targeted delivery of Sb to cancer cells can potentially reduce the level of Akt, Bcl2, IL6, IL17, and other biomolecules which are involved in signaling pathways.[26] These processes, eventually, affect the cell cycle and induce autophagy and apoptotic gene expressions in the cancer cell, and lead to programmed cell death.[27] According to Figure 5A and B, the expression of caspase9 increased about 15 folds in DU145 cells compared with the control group while its expression decreased up to 1.5 fold in PC3 cells (as FA-receptor negative control). The caspase9 gene could induce apoptosis in prostate cancer cells dependent on mitochondrial cytochrome c release pathways through
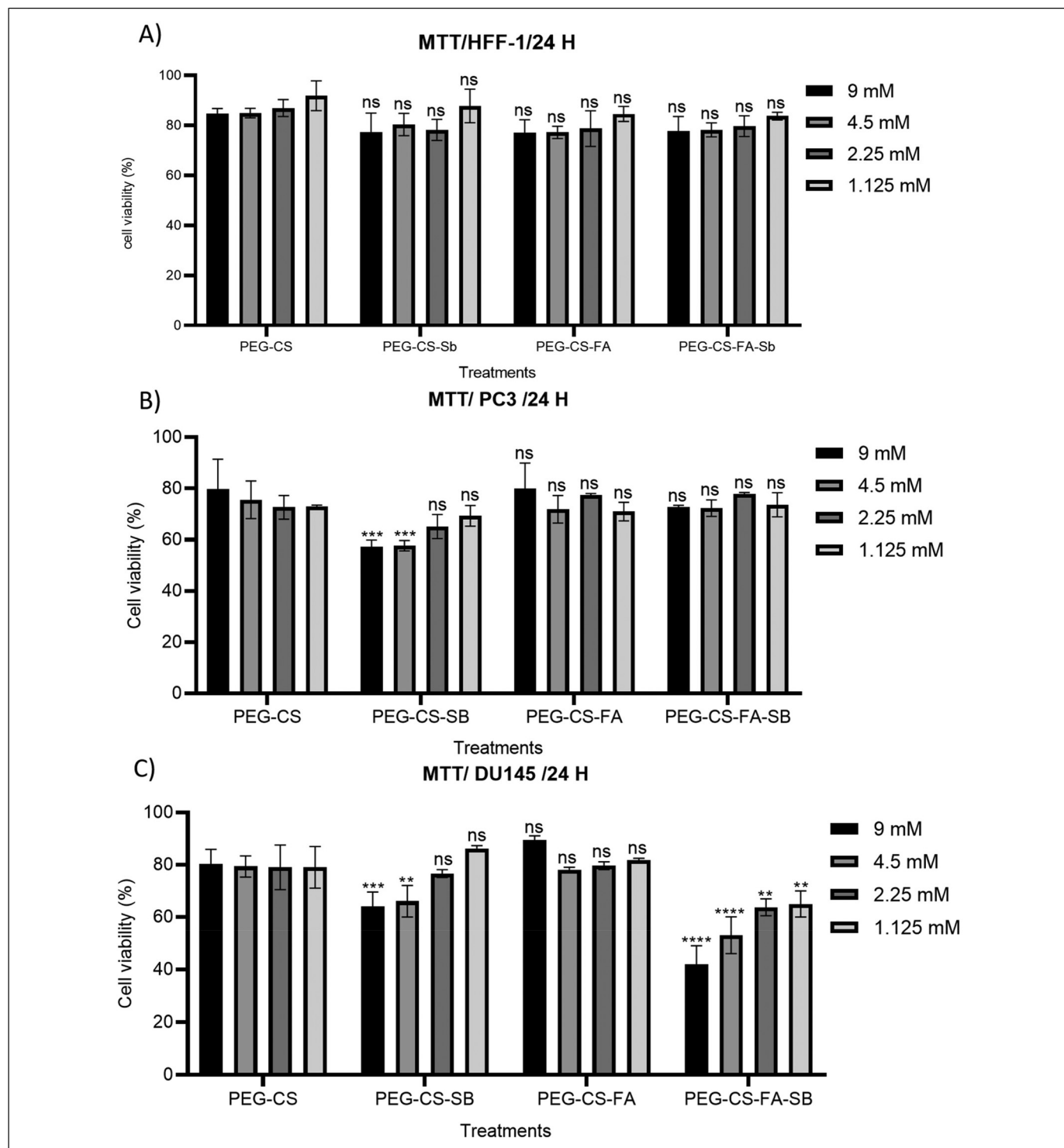
Figure 4. Effects of PEG-CS, PEG-CS-Sb, PEG-CS-FA, PEG-CS-FA-Sb nano-conjugates on cell viability of HFF-1 normal cell lines (A), human PC3 (B), and DU145 (C) prostate cancer after 24 h of treatment with various concentrations (1.125, 2.25, 4.5, and 9 mM). The significant prostate cancer cell growth suppression potency is exhibited for the PEG-CS-FA-Sb sample. As shown, the low cytotoxicity is earned for PEG-CS and PEG-CS-FA nano-complex as biocompatible nanocarriers, which is indicating excellent biocompatibility, biosafety, and biodegradability of the synthetic nano-complex. In all plots, data are represented as mean ± standard deviation (n = 3). Statistical significance was calculated by one-way ANOVA analysis of variance and Turkey's multiple comparison test. P-value < .0001 was considered statistically significant between nano-complexes and mimics.
Abbreviations: CS, chitosan; PEG, polyethylene glycol; Sb, sodium butyrate; FA, folic acid.
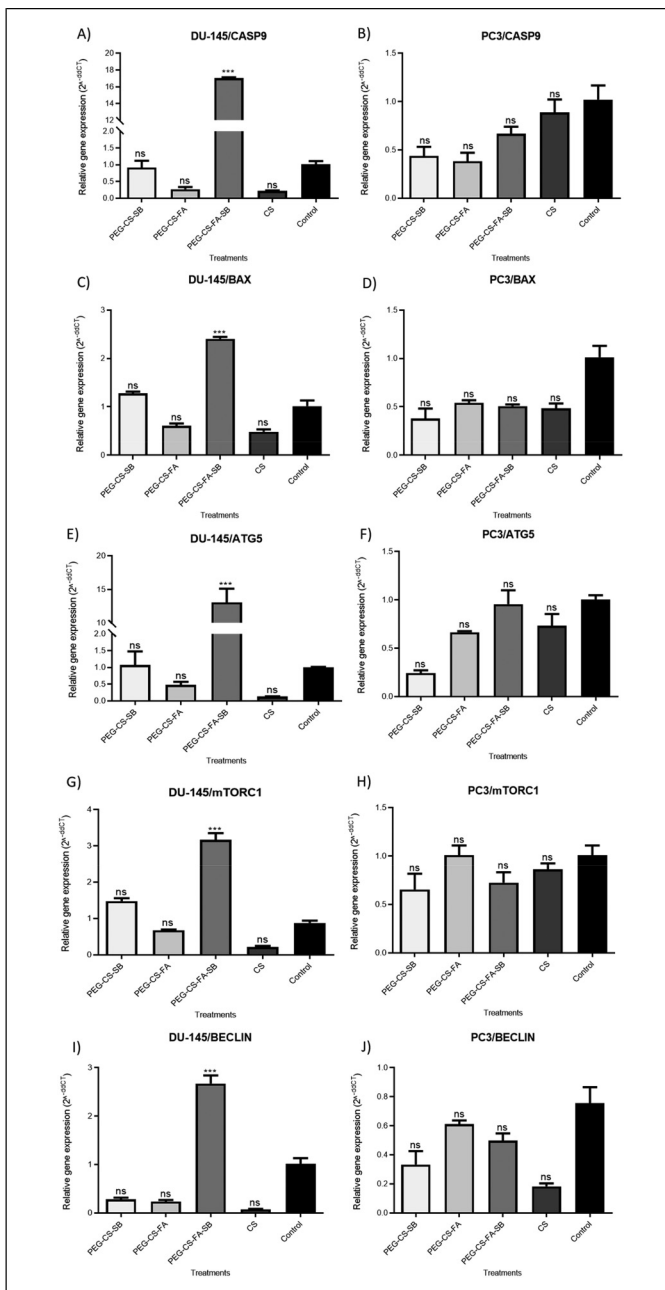
Figure 5. The expression level of apoptotic (Caspase-9, BAX) and autophagy (ATG5, BECLIN1, and mTORC1) genes after 5 h of treatment with 9 mM (IC_{50}) of nano-complexes (PEG-CS, PEG-CS-Sb, PEG-CS-FA, and PEG-CS-FA-Sb) in human PC3 and DU145 prostate cancer cells. The outputs depict that PEG-CS-FA-Sb nano-complex leads to inducing the overexpression of caspase9 (relatively 15 folds compared with control) (A), BAX (2.5 folds) (C), ATG5 (11 folds) (E), mTORC1 (3 folds) (G), and BECLIN1 (2 folds) (I) genes in DU145 cells (as FA-receptor positive) that confirms the potency of nano-complex in inducing programmed cell death. In all plots, data are represented as mean ± standard deviation (n = 3). Statistical significance was calculated by one-way ANOVA analysis of variance and Turkey's multiple comparison test. P-value < .0001 was considered statistically significant between nano-complexes and mimics.

Abbreviations: CS, chitosan; PEG, polyethylene glycol; Sb, sodium butyrate; FA, folic acid.

chromatin condensation and DNA fragmentation.[42] BAX gene expression is also raised more than 2.5 folds in comparison to control in FA-receptor positive DU145 cells (Figure 5C), whereas its expression does not show any enhancement in PC3 (Figure 5D) cells. BAX results in apoptosis via puncturing the outer membrane of mitochondria.[43] Moreover, the expression of these 2 genes did not rise in both cancer cells after treatment with PEG-CS-Sb which further approves the targeted internalization of the nanocarrier. These data have been presenting the effective internalization of PEG-CS-FA-Sb nano-complex in FA-receptor expressing cells and efficient drug delivery to prostate cancer cells. Also, expression of ATG5, BECLIN1, and mTORC1 autophagy genes in DU145 cancer cells (Figure 5E, G and I) was increased by approximately 11 folds, 2 folds, and 3 folds compared with control after treatment with PEG-CS-FA-Sb nano-complex while their expression values were as same as control groups in PC3 cells (Figure 5F, H and J). Expression of these autophagy genes is linked to the expression of apoptotic genes which leads to the localization of autophagy proteins in the membrane of various vesicles and subsequently, induces the disintegration of cancer cells. For instance, the expression of BECLIN1 and mTORC1 can control the localization of autophagy proteins in autophagy vesicles and influence the function of various carcinogenic and metabolic processes such as autophagy pathways in cancer cells.[44] mTORC1 serves as a main regulator of autophagy and its inhibition is crucial for initiating the autophagy process. mTORC1 can phosphorylate specific types of protein in the autophagy process and change their functions, enhance proteasomal degradation, and regulate acetylation of proteins that subsequently, lead to autophagy.[45] On the other hand, BECLIN1 acts as a master regulator of autophagy machinery via activation of Vps34 that modulates through transcriptional regulation, posttranslational modification, and interaction with BECLIN1 binding proteins. BECLIN1 can also bind to Bcl-2/XL which negatively regulates the autophagy process. Our autophagy outputs for PC3 cells are inconsistent with research that has been conducted by Zheng et al[46] in which they applied CS nano-complexes for the delivery of gefitinib and chloroquine to cancer cells while the reverse is true for DU145 cells (increased values of autophagy gene) which indicates efficient internalization of FA-targeted CS nano-complex results in autophagy in FA-receptor positive cells. In another research by Li et al,[47] CS/Alginate-Fe_3O_4 nano-complex was used for the evaluation of the chemosensitization of multidrug-resistant gastric carcinoma in mice and autophagy's role in that process. They indicated that CS-based nanocarriers can promote the autophagy pathway and upregulate ATG5 expression.

Cell Cycle Arrest Assay

The cell growth inhibitory effects of PEG-CS-FA and PEG-CS-FA-Sb nano-complexes were further examined via evaluation of the progression of the cell cycle arrests in human PC3 and DU145 prostate cancer cells.[48] Figure 6
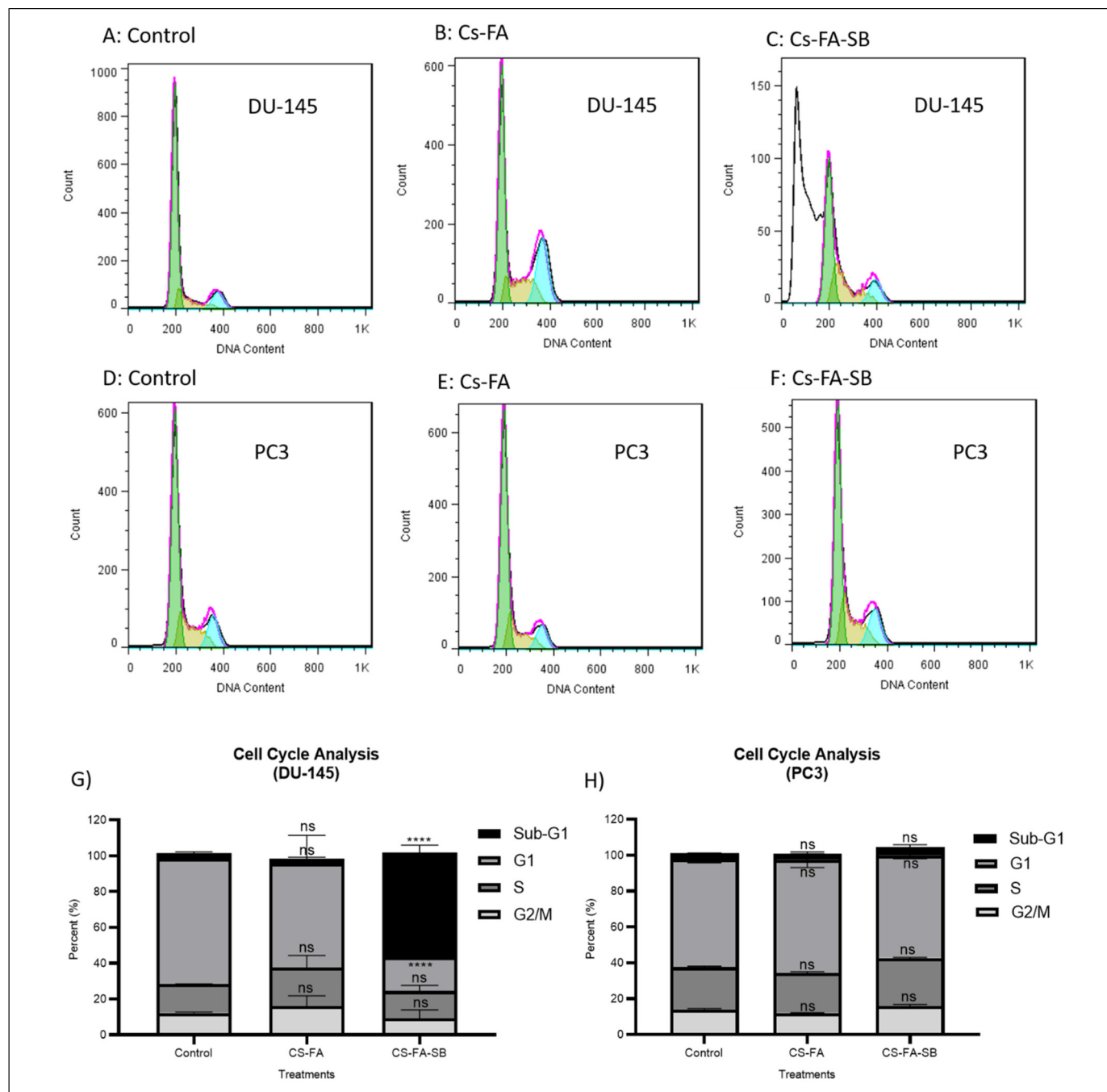
Figure 6. Cell cycle arrest assay outputs on DU145 (A-C) and PC3 (D-F) cells after treatment with 9 mM of FA-CS-PEG and PEG-CS-FA-Sb nano-complexes. As shown, the PEG-CS-FA-Sb sample depicts more than 50% of cell cycle arrest compared with control which is due to FA-receptor-mediated internalization of synthetics and drug release in the cytoplasm of DU145 cancer cells (G). Moreover, PC3 cells as FA-receptor negative cells do not enter the Sub-G1 phase which approves the targeting potency of FA-decorated nano-complex in FA-expressing cancer cells (H). On the other hand, FA-CS-PEG formulation does not show considerable cell suppression in cancer cells which verifies the biocompatibility and biodegradability of the nanocarrier. In all plots, data are represented as mean ± standard deviation (n = 3). Statistical significance was calculated by one-way ANOVA analysis of variance and Turkey's multiple comparison test. *P*-value < .0001 was considered statistically significant between nano-complexes and mimics.
Abbreviations: CS, chitosan; PEG, polyethylene glycol; Sb, sodium butyrate; FA, folic acid.

presents the results of this test. According to results, less than 5% and 8% of PC3 cancer cells (Figure 6H) were in the Sub-G1 phase (indicator to cell suppression and apoptosis) after treatment with 9 mM of PEG-CS-FA, and

PEG-CS-FA-Sb nano-complexes, respectively, which is due to a lack of FA-receptor in PC3 cancer cells and low internalization values. The surface modification of CS with PEG biopolymer and FA biomolecule can noticeably increase different
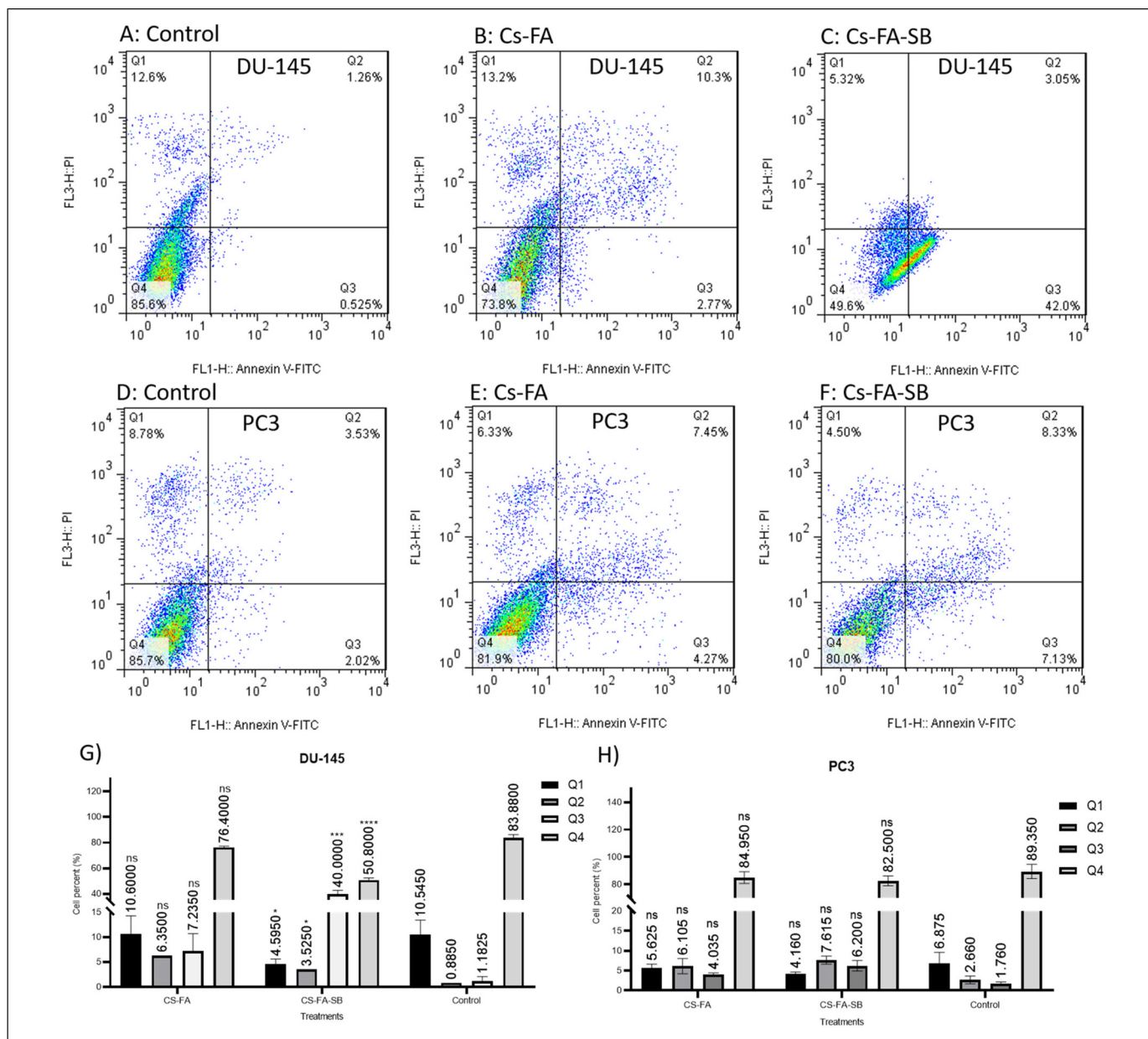
Figure 7. Apoptosis plots of DU145 (A-C) and PC3 (D-F) prostate cancer cells after treatment with 9 mM of PEG-CS-FA and PEG-CS-FA-Sb formulations applying Annexin VFITC and PI staining. As presented, the PEG-CS-FA-Sb sample revealed 45.05% apoptosis on DU145 cells (G) which is higher than that in PC3 cancer cells (15.45%) (H). The live-cell values were 49.8% and 80.0% in DU145 and PC3 cells, respectively. These data depict efficient cancer cell growth suppression after treatment with FA-decorated and Sb-loaded nanocarrier which is favorable for targeted cancer therapy. The Q1, Q2, Q3, and Q4 quarters demonstrate the values of necrotic, late apoptosis, early apoptosis, and live cells, respectively. In all plots, data are represented as mean ± standard deviation (n = 3). Statistical significance was calculated by one-way ANOVA analysis of variance and Turkey's multiple comparison test. *P*-value < .0001 was considered statistically significant between nano-complexes and mimics.

Abbreviations: CS, chitosan; PEG, polyethylene glycol; Sb, sodium butyrate; FA, folic acid.

properties of nanocarrier like biocompatibility and biodegradability, stability, EPR effect, controlled drug release, and so forth which is in favor of novel delivery systems.[21,24] Meanwhile, the PEG-CS-FA-Sb nano-complex depicts more than 50% of cell cycle arrest compared with the control that is owing to FA-receptor-mediated internalization of synthetics

and efficient drug release in the cytoplasm of DU145 cancer cells (Figure 6G). This kind of Sb delivery to cancer cells can suppress VEGF through HDACs and results in protein kinase B (Akt)-mediated suppression of cell-cycle in G2/M and subsequently triggered cell apoptosis.[27] These results are in line with our MTT assay data and as well as the finding of Kumar et al,[29]

in which CS-coated-trans resveratrol and ferulic acid-loaded solid lipid nanoparticles conjugated with FA are used for inhibition of colon cancer. The results of our research were in line with the outputs of a study by Kumar et al[29] in which resveratrol and ferulic acid therapeutics were transported to colon cancer cells via a modified CS nano-complex. They indicated that 51.9% and 68.6% of cancer cells were in the Sub-G1 phase after treatment with resveratrol-loaded and resveratrol + ferulic acid-loaded CS-FA nano-complexes which is similar to the results of DU145 cancer cells in our study. Also, in comparison to Li et al's work,[47] where CS/Alginate-Fe_3O_4 nano-complex was used for suppression of cancer cells, our formulation has indicated about 1.3 folds better performance than their sample.

Apoptosis Assay

To further evaluation of the cell growth inhibition capability of synthetics, the apoptosis assay was performed on PC3 and DU145 cancer cells with 9 mM of PEG-CS-FA and PEG-CS-FA-Sb nano-complexes, respectively (Figure 7). To follow this, the double staining assay based on annexin V-FITC (can bind to phosphatidylserine [PS]) and PI (intercalates in the DNA fragmentations) was used. This approach can follow the translocation of inner plasma membrane phospholipid PSs to the outer layer of the membrane in apoptotic cells.[49] According to the results indicated in Figure 7, both prostate cancer cells did not demonstrate considerable apoptosis (Q2: late apoptosis; Q3: early apoptosis) and necrosis (Q1) after treatment with PEG-CS-FA sample and about 73% (DU145) (Figure 7A to C) and 81% (PC3) (Figure 7D to F) of cells were live (Q4) which due to its biocompatibility and biodegradability. A low value of live cell DU145 cells compared with PC3 cells could be owing to high internalization PEG-CS-FA nano-complex which, in turn, can result in overdoes of these cells and cell death. On the other hand, the PEG-CS-FA-Sb nano-complex exhibited 45.05% apoptosis on DU145 cells (Figure 7G) which is higher than that in PC3 cancer cells (15.45%) (Figure 7H). The live-cell values were 49.8% and 80.0% in DU145 and PC3 cells. These data have been potentially indicating that targeted PEG-CS-FA-Sb nano-complexes can induce programmed cell death in prostate cancer cells which is a promising nanocarrier for efficient targeted cancer therapy.[18] The results of this assay are inconsistent with cell cycle arrest and MTT assay and further, confirm the ability of nano-complex in the suppression of cancer cells. Our data is also in line with the findings of Jin et al,[50] who developed an FA-functionalized CS nano-complex for targeted delivery of ursolic acid to breast cancer in vivo. The findings of our research are also in line with a study by Zheng et al[46] in which gefitinib- and chloroquine-loaded and antibody-conjugated CS nano-complex were used for inhibition of cancer cells and relatively 54% apoptosis was attained for co-leaded nano-complex, whereas it was less than 46% (like our nano-complex performance on DU145 cells) apoptosis for nanocarriers that loaded with separate therapeutics.

Conclusion

In this research, we have successfully developed the PEG-modified and FA-decorated CS nano-complex as a promising drug delivery system for the delivery of Sb to prostate cancer cells. The synthetics were qualified and quantified via analytical devices including FT-IR, DLS, SEM, and TEM. The nanometric size with appropriate drug entrapment efficiency and controlled drug release in the pH of normal microenvironment were observed for PEG-CS-FA-Sb nano-complex which are the most important aspects for nanoparticle-based drug delivery systems. Then, some biomedical test like MTT assay, gene expression, and cell cycle arrest apoptosis was applied for scrutinizing the prostate cancer cell growth suppression ability of nano-complex. Outputs have noticeably verified the potential performance of PEG-CS-FA-Sb nano-complex in the inhibition of cancer cells. Our outputs suggest that synthesized nano-complex would be beneficial for practical in vivo studies in the future since all parts of this nanocomposite are practically assembled from biodegradable and biocompatible materials that are non-toxic and efficiently cancerous suppressors. These targeted nanocomposites can effectively target folic acid receptors and could be a good candidate for targeted drug delivery of Folic acid receptor-positive cancers. The limitation of this study is detecting Sb by HPLC which is time-consuming and expensive. Moreover, the chitosan nanoparticles have a vast range in diameter and lack long stability. However, PEGylation can overcome this problem to a large extent.

ORCID iDs

Soroush Alazmani https://orcid.org/0000-0003-1411-4722
Sepideh Khaleghi https://orcid.org/0000-0002-1817-3116

Supplemental Material

Supplemental material for this article is available online.

References

1. Licciardi M, Paolino D, Celia C, Giammona G, Cavallaro G, Fresta M. Folate-targeted supramolecular vesicular aggregates based on polyaspartyl-hydrazide copolymers for the selective

delivery of antitumoral drugs. *Biomaterials*. 2010 1;31(28):7340-7354.

2. Yousefi M, Narmani A, Jafari SM. Dendrimers as efficient nano-carriers for the protection and delivery of bioactive phytochemicals. *Adv Colloid Interface Sci*. 2020;278(1):102125.

3. Kumari R, Sunil D, Ningthoujam RS. Hypoxia-responsive nanoparticle based drug delivery systems in cancer therapy: an up-to-date review. *J Control Release*. 2020;319(10):135-156.

4. Narmani A, Farhood B, Haghi-Aminjan H, et al. Gadolinium nanoparticles as diagnostic and therapeutic agents: their delivery systems in magnetic resonance imaging and neutron capture therapy. *J Drug Deliv Sci Technol*. 2018;44(1):457-466.

5. Narmani A, Yavari K, Mohammadnejad J. Imaging, biodistribution and in vitro study of smart ^{99m}Tc-PAMAM G4 dendrimer as novel nano-complex. *Colloids Surf, B*. 2017;159(1):232-240.

6. Chen C, Yu Y, Wang X, Shi P, Wang Y, Wang P. Manipulation of pH-sensitive interactions between podophyllotoxin-chitosan for enhanced controlled drug release. *Int J Biol Macromol*. 2017;95(1):451-461.

7. Yao R, Han D, Sun X, et al. Histone deacetylase inhibitor sodium butyrate suppresses cell proliferation and induces apoptosis by targeting p21 in multiple myeloma. *Am J Transl Res*. 2017;9(11):4994-5002.

8. Donohoe D.R., Garge N., Zhang X., W., et al (2011) The microbiome and butyrate regulate energy metabolism and autophagy in the mammalian colon, *Cell Metab* 4;13(5) 517-526.

9. Chen J, Zhao KN, Vitetta L. Effects of intestinal microbial-elaborated butyrate on oncogenic signaling pathways. *Nutrients*. 2019 7;11(5):1026.

10. Calcinotto A, Brevi A, Chesi M, et al. Microbiota-driven interleukin-17-producing cells and eosinophils synergize to accelerate multiple myeloma progression. *Nat Commun*. 2018 3;9(1):4832.

11. Zeng H, Briske-Anderson M. Prolonged butyrate treatment inhibits the migration and invasion potential ofHT1080 tumor cells. *J Nutr*. 2005 1;135(2):291-295.

12. Luo S, Li Z, Mao L, Chen S, Sun S. Sodium butyrate induces autophagy in colorectal cancer cells through LKB1/AMPK signaling. *J Physiol Biochem*. 2019;75(15):53-63.

13. Ali I, Wani WA, Saleem K, Wesselinova D. Syntheses, DNA binding and anticancer profiles of L-glutamic acid ligand and its copper (II) and ruthenium (III) complexes. *Med Chem*. 2013;9(1):11-21.

14. Ali I, Wani WA, Haque A, Saleem K. Glutamic acid and its derivatives: candidates for rational design of anticancer drugs. *Future Med Chem*. 2013;5(8):961-978.

15. Hussain A, Oves M, Alajmi MF, et al. Biogenesis of ZnO nanoparticles using *Pandanus odorifer* leaf extract: anticancer and antimicrobial activities. *RSC Adv*. 2019;9(27):15357-15369.

16. Saleem K, Wani WA, Haque A, et al. Synthesis, DNA binding, hemolysis assays and anticancer studies of copper (II), nickel (II) and iron (III) complexes of a pyrazoline-based ligand. *Future Med Chem*. 2013;5(2):135-146.

17. Koo H, Min KH, Lee SC, et al. Enhanced drug-loading and therapeutic efficacy of hydrotropic oligomer conjugated glycol chitosan nanoparticles for tumor-targeted paclitaxel delivery. *J Control Release*. 2013 28;172(3):823-831.

18. Narmani A, Arani MAA, Mohammadnejad J, et al. Breast tumor targeting with PAMAM-PEG-5FU-^{99m}Tc as a new therapeutic nanocomplex: in in-vitro and in-vivo studies, *Biomed Microdevices*. 2020;22(2):31.

19. Luo Y, Teng Z, Li Y, Wang Q. Solid lipid nanoparticles for oral drug delivery: chitosan coating improves stability, controlled delivery, mucoadhesion and cellular uptake, *Carbohydr Polym*. 2015;122(20):221-229.

20. Nam HY, Kwon SM, Chung H, et al. Cellular uptake mechanism and intracellular fate of hydrophobically modified glycol chitosan nanoparticles. *J Control Release*. 2009;135(3):259-267.

21. Rezvani M, Mohammadnejad J, Narmani A, Bidaki K. Synthesis and in vitro study of modified chitosan polycaprolactam nanocomplex as delivery system. *Int J Biol Macromol*. 2018;113(1): 1287-1293.

22. Xie Y, Qiao H, Su Z, Chen M, Ping Q, Sun M. PEGylated carboxymethyl chitosan/calcium phosphate hybrid anionic nanoparticles mediated hTERT siRNA delivery for anticancer therapy. *Biomaterials*. 2014;35(27):7978-7991.

23. Pillai JJ, Thulasidasan AKT, Anto RJ, Devika NC, Ashwanikumar N, Kumar GV. Curcumin entrapped folic acid conjugated PLGA–PEG nanoparticles exhibit enhanced anticancer activity by site specific delivery. *RSC Adv*. 2015;5(32):25518-25524.

24. Mortezaee K, Narmani A, Salehi M, Bagheri H, Farhood B, Haghi-Aminjan H. Synergic effects of nanoparticles-mediated hyperthermia in radiotherapy/chemotherapy of cancer. *Life Sci*. 2021;269(15):119020.

25. Li C, Li H, Wang Q, et al. pH-sensitive polymeric micelles for targeted delivery to inflamed joints. *J Control Release*. 2017;246(28):133-141.

26. Narmani A, Rezvani M, Farhood B, et al. Folic acid functionalized nanoparticles as pharmaceutical carriers in drug delivery systems. *Drug Dev Res*. 2019;80(4):404-424.

27. Lu Y, Low PS. Folate-mediated delivery of macromolecular anticancer therapeutic agents. *Adv Drug Deliv Rev*. 2002.

28. Faramarzi N, Mohammadnejad J, Jafary H, Narmani A, Koosha M, Motlagh B. Synthesis and in vitro evaluation of tamoxifen-loaded gelatin as effective nano-complex in drug delivery systems. *Int J Nanosci*. 2020;19(5):2050002.

29. Kumar CS, Thangam R, Mary SA, Kannan PR, Arun G, Madhan B. Targeted delivery and apoptosis induction of trans-resveratrol-ferulic acid loaded chitosan coated folic acid conjugate solid lipid nanoparticles in colon cancer cells. *Carbohydr Polym*. 2020;231(1):115682.

30. Bandara S, Carnegie C, Johnson C, Akindoju F, Williams E, Swaby JM. Synthesis and characterization of zinc/chitosan-folic acid complex. *Heliyon*. 2018 1;4(8):e00737.

31. Parveen S, Sahoo SK. Long circulating chitosan/PEG blended PLGA nanoparticle for tumor drug delivery. *Eur J Pharmacol*. 2011;670(2-3):372-383.

32. Nag M, Gajbhiye V, Kesharwani P, Jain NK. Transferrin functionalized chitosan-PEG nanoparticles for targeted delivery of paclitaxel to cancer cells. *Colloids Surf, B*. 2016;148(1):363-370.

33. Chalati T, Horcajada P, Gref R, Couvreur P, Serre C. Optimisation of the synthesis of MOF nanoparticles made of flexible porous iron fumarate MIL-88A. *J Mater Chem*. 2011;21(7):2220-2227.

34. Kanth V, Kajjari P, Madalageri P, Ravindra S, Manjeshwar L, Aminabhavi T. Blend hydrogel microspheres of carboxymethyl chitosan and gelatin for the controlled release of 5-fluorouracil. *Pharmaceutics*. 2017;9(2):13.

35. Jiang K, Chi T, Li T, et al. A smart pH-responsive nano-carrier as a drug delivery system for the targeted delivery of ursolic acid: suppresses cancer growth and metastasis by modulating P53/MMP-9/PTEN/CD44 mediated multiple signaling pathways. *Nanoscale*. 2017;9(27):9428-9439.

36. Kadare P, Maposa P, Dube A, Maponga CC. Encapsulation of isoniazid in chitosan-gum arabic and poly (lactic-co-glycolic acid) PVA particles to provide a sustained release formulation. *J Pharmaceu Pharmacol*. 2014(1):01-06.

37. Zheng H, Zhang Y, Liu L, et al. One-pot synthesis of metal-organic frameworks with encapsulated target molecules and their applications for controlled drug delivery. *J Am Chem Soc*. 2016;138(3):962-968.

38. Basavaraj S, Betageri GV. Improved oral delivery of resveratrol using proliposomal formulation: investigation of various factors contributing to prolonged absorption of unmetabolized resveratrol. *Expert Opin Drug Deliv*. 2014;11(4):493-503.

39. Xie P, Du P, Li J, Liu P. Stimuli-responsive hybrid cluster bombs of PEGylated chitosan encapsulated DOX-loaded superparamagnetic nanoparticles enabling tumor-specific disassembly for on-demand drug delivery and enhanced MR imaging. *Carbohydr Polym*. 2019;205(1):377-384.

40. Khan MM, Madni A, Filipczak N, et al. Folate targeted lipid chitosan hybrid nanoparticles for enhanced anti-tumor efficacy. *Nanomedicine*. 2020;28(1):102228.

41. Inphonlek S, Sunintaboon P, Léonard M, Durand A. Chitosan/carboxymethylcellulose-stabilized poly(lactide-co-glycolide) particles as bio-based drug delivery carriers. *Carbohydr Polym*. 2020;242(15):116417.

42. Jiao C, Chen W, Tan X, et al. *Ganoderma lucidum* spore oil induces apoptosis of breast cancer cells in vitro and in vivo by activating caspase-3 and caspase-9. *J Ethnopharmacol*. 2020;247(30):112256.

43. Lindenboim L, Grozki D, Amsalem-Zafran AR, et al. Apoptotic stress induces bax-dependent, caspase-independent redistribution of LINC complex nesprins. *Cell Death Discov*. 2020;6(1):90.

44. Zou M, Lu N, Hu C, et al. Beclin 1-mediated autophagy in hepatocellular carcinoma cells: implication in anticancer efficiency of oroxylin A via inhibition of mTOR signaling. *Cell Signal*. 2012;24(8):1722-1732.

45. Dossou AS, Basu A. The emerging roles of mTORC1 in macro-managing autophagy. *Cancers (Basel)*. 2019;11(10):1422.

46. Zheng Y, Su C, Zhao L, Shi Y, Mab MDR1-modified chitosan nanoparticles overcome acquired EGFR-TKI resistance through two potential therapeutic targets modulation of MDR1 and autophagy. *Nanobiotechnol*. 2017;15(1):66.

47. Li X, Feng J, Zhang R, et al. Quaternized chitosan/alginate-Fe_3O_4 magnetic nanoparticles enhance the chemosensitization of multidrug-resistant gastric carcinoma by regulating cell autophagy activity in mice. *J Biomed Nanotechnol*. 2016;12(5):948-961.

48. Thangam R, Senthilkumar D, Suresh V, Sathuvan M, Sivasubramanian S, Pazhanichamy K. Induction of ROS-dependent mitochondria- mediated intrinsic apoptosis in MDA-MB-231 cells by glycoprotein from *Codium decorticatum*. *J Agric Food Chem*. 2014;62(15):3410-3421.

49. Wang L, Zhou B–B, Yu K, et al. Novel antitumor agent, trilacunary keggin-type tungstobismuthate, inhibits proliferation and induces apoptosis in human gastric cancer SGC-7901 cells. *Inorg Chem*. 2013;52(9):5119-5127.

50. Jin H, Pi J, Yang F, et al. Folate chitosan nanoparticles loaded with ursolic acid confer anti-breast cancer activities in vitro and in vivo. *Sci Rep*. 2016;6(1):30782.